Journal of Applied Polymer Science

Investigation on the Morphology and Tensile Behavior of β-Nucleated Isotactic Polypropylene with Different Stereo-Defect Distribution

Hongmei Peng, Bin Wang, Jinggang Gai, Jinyao Chen, Feng Yang, Ya Cao, Huilin Li, Jian Kang, Ming Xiang

State Key Laboratory of Polymer Materials Engineering, Polymer Research Institute of Sichuan University, Chengdu, Sichuan 610065, People's Republic of China

Correspondence to: J. Kang (E-mail: jiankang@scu.edu.cn) or M. Xiang (E-mail: xiangming45@hotmail.com).

ABSTRACT: Large amount of work has been published on the tacticity-properties relationship of isotactic polypropylene (iPP). However, the stereo-defect distribution dependence of morphology and mechanical properties of β-nucleated iPP (β-iPP) is still not clear. In this study, two different iPP resins (PP-A and PP-B) with similar average isotacticity but different uniformities of stereo-defect distribution were selected, their β-iPP injection molding specimens were prepared, and the morphology evolution and tensile behaviors were studied by means of differential scanning calorimetry (DSC), 2D wide-angle X-ray diffraction (2D-WAXD) and scanning electron microscope (SEM). DSC results showed that with the same concentration of β-nucleating agent (0.3 wt % WBG-II), PP-B with more uniform stereo-defect distribution exhibited more amount of β-phase than that of PP-A with less uniform stereo-defect distribution, indicating that PP-B is more favorable for the formation of β-phase. SEM results showed that PP-B formed more amount of β-crystals with relatively high structural perfection, while in PP-A a mixed morphology of α- and β-phase with obviously higher amount of structural imperfection emerges. The results of room-temperature tensile test indicated that the yield peak width of PP-B was obviously wider, and the elongation at break of PP-B was higher than that of PP-A, showing a better ductile of PP-B. The morphology evolution results of SEM, 2D-WAXD and DSC suggest that, a combination of lamellar deformation and amorphous deformation occurred in PP-A, while only amorphous deformation mainly took place in PP-B, which was thought to be the reason for the different tensile behaviors of the samples. In the production of β-PP products via injection molding, the uniformity of stereo-defect distribution was found to be an important factor. PP with more uniform distribution of stereo-defect favors the formation of large amount of β-phase with high perfection, which exhibit superior ductile property. The related mechanism was discussed. © 2013 Wiley Periodicals, Inc. J. Appl. Polym. Sci. **2014**, *131*, 40027.

KEYWORDS: differential scanning calorimetry; properties and characterization; resins; structure–property relations; phase behavior

Received 4 August 2013; accepted 30 September 2013

DOI: 10.1002/app.40027

INTRODUCTION

Isotactic polypropylene (iPP) is one of the most widely used commercial polymer materials owning to its low manufacturing cost and rather versatile properties. It is a typical polymorphic plastic with several crystal modifications: monoclinic (α), trigonal (β), orthorhombic (γ) form, and smectic mesophase (intermediate state between ordered and amorphous phase), all sharing the same threefold conformation but with different spatial arrangements of iPP chains in the crystal lattice.[1–8] It is accepted that the α-form is the thermodynamically stable one, and the commercial polypropylene grades have crystallized mostly in the α-form under the usual industrial thermal conditions. The γ-form is preferentially formed from crystallization under pressure.[9] As the β-form have several advantageous characteristics such as improved impact strength and toughness (ductility), many research groups have focused their interest on the β-iPP.[10–13] A small amount of β-form is found to accompany the α-form under conventional thermal conditions, especially at high supercooling.[14,15] High content of β-form can be obtained under special crystallization conditions[16,17]or by using selective β-crystal nucleating agents.[18–21] The mechanical behavior of a semicrystalline polymer is believed to be strongly affected by the mechanical coupling or stress transmission between crystalline and amorphous structures.[22–27] Luo and his coworkers demonstrated that the connection between crystallites might mainly determine the toughness of iPP instead of the β-crystal content.[28] Shi and his coworkers studied the formation of micropores in β-PP under stretching, and proposed the related mechanism.[29]

During the past decades, the relationship between molecular structure and properties of PP had been extensively studied,[30–33]

© 2013 Wiley Periodicals, Inc.

Table I. Molecular Characteristics of PP-A and PP-B Studied

Sample	Isotacticity (%)[a]	XS (%)[b]	M_w (kg/mol)[c]
PP-A	96.6	3.8	365
PP-B	96.4	3.9	347

[a] Isotacticity were obtained from high temperature ^{13}C NMR at 120°C.
[b] Xylene soluble fraction at room temperature according to ASTM D5492.
[c] Molecular weight and distribution were performed by GPC at 130°C.

and it was found that the thermodynamic, morphological, and mechanical properties of PP strongly depend on the type, content, and distribution of defects generated during synthesis.[34,35] M.R. Nydena[36] used the results of the calculations performed to assign defect-resonance patterns observed in solid-state ^{13}C NMR spectra obtained from the crystalline regions of iPP to help establish the conformational structures of the defect-containing stems. Claudio[37] described the use of a series of catalysts produce iPP with different degrees of stereo regularity, the effect of the presence of rr defects on the polymorphic behavior and mechanical properties of polypropylene was analyzed. Recently, Alamo and coworkers[38,39] demonstrated that, even a small number of stereo-defects can, however, lead to different properties depending on the distribution of the defects along the chain. Our previous work[40] revealed that the stereo-defect distribution, together with the thermal conditions, play an important role in determining the crystallization behavior and morphology of β-PP.

However, as far as we have concerned, little information about the effect of the uniformity of the stereo-defect distribution on the morphology and mechanical performance of β-iPP can be available, which is of great importance for tuning the morphology and properties of the β-iPP products.

In our previous works,[41–43] two iPP samples with different uniformities of stereo-defect distribution were prepared by tuning the polymerization conditions. Their molecular structure, conformational behavior and crystallization behavior were studied. The aim of this study is to further investigate the effect of stereo-defect distribution on the morphology and mechanical properties of the injection molded β-iPP products. Both the influence of stereo-defect distribution and the injection molding process were taken into consideration, the related mechanism were discussed.

EXPERIMENTAL

Materials

The iPP resins used in this study (PP-A and PP-B) were synthesized by two different highly activity supported forth generation Ziegler-Natta ($TiCl_4 = MgCl_2$) catalysts, ZN-A and ZN-B, respectively. The catalytic activity of ZN-A is higher than that of ZN-B. Other polymerization conditions, such as hydrogen concentration, Al/Si ratio, temperature, pressure, of the two polymerization systems were the same. The molecular information of the samples, such as average isotacticity, weight average (M_w) and the content of regular pentads were summarized in Tables I and II. The rare earth β-nucleating agent with the trade name of WBG-II which exhibits very high β-selectivity and efficiency, was kindly supplied by Winner Functional Materials (Foshan, Guangdong, China). The raw WBG-II is a kind of irregular block-like crystal. The single crystal diameter is about tens of nanometers, and most of the agglomerates consist of several crystals. As can be seen from Tables I and II, the average isotacticity and molecular weight of PP-A and PP-B are similar, however, the stereo-defect distribution of PP-B is more uniform than that of PP-A.[42]

Sample Preparation

WBG-II was first melt mixed with iPP in a twin-screw extruder to produce a 1.0 wt % β-nucleating agent masterbatch. The masterbatch was further melt-compounded with fresh iPP to produce β-iPP (pellets) with 0.3 wt % of WBG-II. The screw speed was fixed at 10 rpm, and the processing temperature profile was 170–190°C from hopper to die. Standard ASTM tensile bars of PP-A and PP-B were cast on a Milacron KTEC40 reciprocating screw injection-molding machine in an injection temperature profile of 170–200°C from hopper to nozzle. ASTM dumbbell specimens were injection molded with length 80 mm, width 10 mm, and thickness 4 mm.

Differential Scanning Calorimetry

Thermal properties of specimens were analyzed using a differential scanning calorimeter (DSC), Mettler Toledo DSC1. The thermal behavior of the samples was obtained by heating from 25 to 200°C at a heating rate of 10°C min^{-1} under nitrogen atmosphere (50 mL/min). The deformed regions were taken from the deformed part of the tensile samples. The fraction of β-PP ($K_{\beta\text{-DSC}}$) in the matrix can be calculated from the following equation:

$$K_{\beta\text{-DSC}} = \frac{X_{c\beta}}{X_{c\beta} + X_{c\alpha}} \quad (1)$$

where $X_{c\alpha}$ and $X_{c\beta}$ are the degrees of crystallinity for α-phase and β-phase, respectively.

The degree of crystallinity (X_c) for each sample was calculated by

Table II. Tacticity Results from HRHT ^{13}C NMR Analysis of PP-B and PP-A

	mm			mr			rr		
Sample[a]	mmmm	mmmr	rmmr	mmrr	mmrm + rmrr	rmrm	rrrr	mrrr	mrrm
PP-A	95.07	1.59	0.41	2.12	0.57	0.30	0.61	0.45	0.88
PP-B	94.78	1.47	0.53	2.17	0.71	0.31	0.65	0.48	0.90

[a] Samples were extracted in *n*-heptane for 24 h at desired temperature and then the insoluble fraction was collected and dried for HRHT ^{13}C NMR measurement, to exclude the influence of the atactic fraction.

$$X_c = \frac{\Delta H_m}{\rho \times \Delta H_m^0} \quad (2)$$

where ρ is the weight fraction of iPP in corresponding sample, ΔH_m is the DSC measured value of fusion enthalpy, and ΔH_m^0 is the fusion enthalpy of the completely crystalline iPP. Here, the values of ΔH_m^0 for α- and β-modification are selected as 177.0 and 168.5 J/g,[44] respectively. Since partial β-phase will transform into α-phase during DSC scan, leading to the increase of $X_{c\alpha}$, the fraction of β-phase obtained by DSC measurement will be lower than the actual one in the sample. However, the variation trends of both α-phase and β-phase can be achieved and the data are acceptable to a certain degree.

Tensile Measurement

Uniaxial tensile relaxation tests were performed at room temperature on a testing machine Instron 4302 Tensile Tester (Instron Corp, Canton, MA) according to GB 1040-79. The temperature selected was room temperature (25°C).

Scanning Electron microscopy

A JSM-5900 LV environmental scanning electron microscope was used at an accelerating voltage of 20 kV. Before scanning electron microscope (SEM) characterizations, the surfaces of all the samples were coated with a thin layer of gold by ion sputtering. On the other hand, for characterizing the crystallization structure of the samples, all the samples were etched for 2 h in a solution containing 1.3 wt % potassium permanganate ($KMnO_4$), 32.9 wt % concentrated sulfuric acid (H_2SO_4), and 65.8 wt % concentrated phosphoric acid (H_3PO_4), according to the procedure proposed by Olley and Bassett.[45]

2D-WAXD

Wide angle X-ray diffraction measurement was carried out using a Bruker DX-1000 Discover diffractometer equipped with GADDS (spatial resolution: 105 × 105 μm^2/pixel) as a 2D detector in transmission mode. The X-ray sources (Cu, $\lambda = 0.154$ nm) were provided by 40 K ceramic tubes, and the diffraction peak positions were calibrated with silicon powder ($2\theta > 15°$) and silver behenate ($2\theta < 10°$). The two-dimensional (2D) diffraction patterns were investigated for both the undeformed and deformed regions at room temperature with the exposure time of 300 s. The point-focused X-ray beam of 0.2 mm in diameter was aligned perpendicular to the mechanical stretching direction. The background scattering was recorded and subtracted from the sample patterns. Diffraction profiles were recorded between 4° and 30° with a 0.02° scan.

1D-WAXD profiles were obtained from circularly integrated intensities of 2D-WAXD image patterns acquired. Subsequently, through deconvoluting the peaks of 1D-WAXD profiles, The β-iPP fraction $K_{\beta\text{-WAXD}}$ was calculated from WAXD diffractograms according to the following methodology developed by Turner Jones[46]:

$$K_{\beta\text{-WAXD}} = \frac{H_{300}^{\beta}}{H_{110}^{\alpha} + H_{040}^{\alpha} + H_{130}^{\alpha} + H_{300}^{\beta}} \quad (3)$$

where H_{110}^{α}, H_{040}^{α}, and H_{130}^{α} are the intensities of the (110), (040), and (130) reflections of the α-iPP, respectively, and H_{300}^{β} is the intensity of (300) reflection of β-iPP. Although the $K_{\beta\text{-WAXD}}$ value is the relative measure of the β-iPP amount, it provides at least the variation trend of the β-iPP fraction when the samples are prepared in the same way and the measurement condition is completely same.

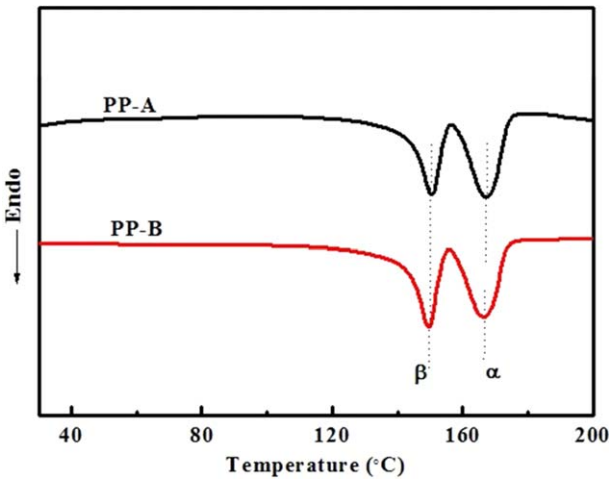

Figure 1. DSC thermograms of melting curves at the heating rate of 10°C/min for PP-A and PP-B injection molding samples containing 0.3 wt % WBG-II. [Color figure can be viewed in the online issue, which is available at wileyonlinelibrary.com.]

RESULTS AND DISCUSSION

Analysis of the Injection Molding Samples

DSC Analysis. Figure 1 exhibits the melting behaviors of PP-A and PP-B injection molding samples with 0.3 wt % WBG-II. After introducing the WBG-II, two predominated fusion peaks are observed at approximate 150–153°C and 164.5–168.3°C (shown as β and α, respectively), indicating the fusion of β-phase and α-phase, respectively.[47] According to the eqs (1) and (2), the $K_{\beta\text{-DSC}}$ of PP-A and PP-B are 47.5 and 56.9%, respectively, indicating that when adding the same concentration of WBG-II, more amount of β-phase is formed in PP-B compared with PP-A.

Wide-Angle X-Ray Diffraction. It is known that the results of DSC of β-PP are usually misleaded by a β-α recrystallization during heating process. Since the WAXD is performed under room temperature, the confusion of β-α phase transformation can be excluded. To understand fully, 2D-WAXD is performed on the injection-molded samples of PP-A and PP-B, the obtained 2D-WAXD, 1D-WAXD patterns are shown in Figures 2 and 3, respectively. The corresponding crystalline structure parameters are listed in Table III.

As can be seen from Figures 2 and 3 and Table III, three nearly isotropic diffraction rings are detected in PP-A and PP-B, which are indexed as (110)α, (300)β, (111)α, respectively (from inner to outer). Compared with PP-A, the intensities of the (300)β ring (second inner ring) in Figure 2 and the diffraction peak located 2θ of about 15.8° are all higher than that of PP-A, indicating that the proportion of β-phase of PP-B is higher than that of PPA. The d-spacing and the crystallite size L of PP-B are all larger than that of PP-A, indicating that the crystals formed in PP-A are smaller, which pack more compactly.

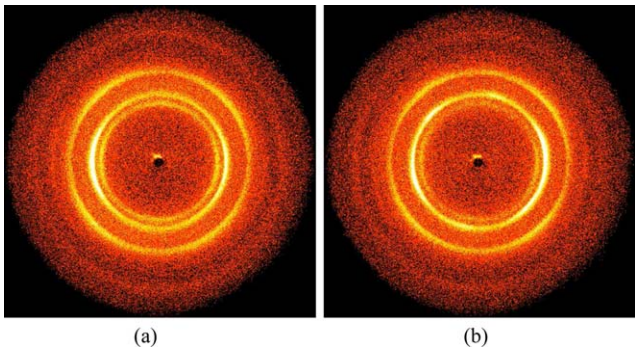

Figure 2. 2D-WAXD patterns of the injection-molded samples of (a) PP-A and (b) PP-B with 0.3 wt % WBG-II. [Color figure can be viewed in the online issue, which is available at wileyonlinelibrary.com.]

It should be noted that according to the calculation of $K_{\beta\text{-WAXD}}$, it is found that the β-fraction of PP-B (69.8%) is 17% higher than that of PP-A (53.4%). This difference in β-content is obviously larger than the $K_{\beta\text{-DSC}}$ measured by DSC above, which might be attributed to the influence of β-α recrystallization during heating.

SEM Observation. To obtain direct morphology information of the samples, SEM analysis is carried out on cryogenic fracture surfaces obtained from the raw dumbbell specimens, perpendicular to the melt flow direction. After etching, they are coated with gold and examined in SEM to study the crystals morphology. The obtained images are presented in Figure 4. As can be clearly seen from Figure 4, for PP-A, wide alternant distribution of darker area (α-phase) and lighter areas (β-phase)[48–51] can be observed, indicating the coexist of large amount of both α- and β-phase. Meanwhile, the SEM image of PP-B is mainly filled up with lighter areas, which contains the substructure of stacked lamellaes, indicating that in PP-B an obviously larger amount of β-phase has formed. This result is in accord with the WAXD analysis above.

On the other hand, many voids and "defects" can be observed in PP-A, which might be defective structures (i.e., the crystals with low perfection or amorphous). These defective structures are removed during the etching process. Interestingly, much fewer "defects" can be observed in PP-B, suggesting that under the injection molding process and the influence of WBG-II, PP-B has obviously higher proportion of β-phase and less amount of defective structures.

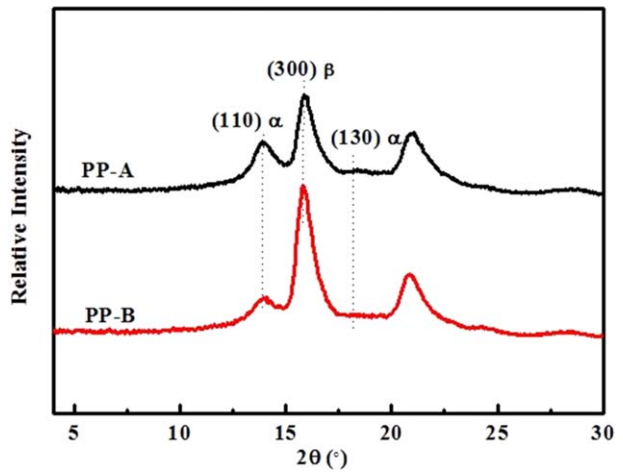

Figure 3. 1D-WAXD patterns of the injection-molded samples of PP-A and PP-B containing 0.3 wt % WBG-II. [Color figure can be viewed in the online issue, which is available at wileyonlinelibrary.com.]

Tensile Behavior

The above analysis of the injection-molded specimens of PP-A and PP-B with 0.3 wt % WBG-II indicate that, the uniformity of stereo-defect distribution greatly influences the β-phase content, thermal stability and morphology of the β-PP samples during injection molding, which might further influence their tensile behavior and morphology evolution behavior. Therefore, tensile experiment at room temperature (25°C) is performed. Figure 5 shows the stress–strain curves of the samples at a crosshead speed of 50 mm/min (strain rates 0.01/s). The obtained parameters are listed in Table IV.

As can be seen from Figure 5 and Table IV, the tensile behavior of PP-A and PP-B with 0.3 wt % WBG-II are quite different from each other. The yield strength and elastic modulus of PP-A are all higher than that of PP-B, meanwhile, the yielding peak width of PP-A is obviously narrower than that of PP-B, which might be attributed to the higher proportion of α-phase in PP-A. Since in PP-B the majority of crystal is β-modification, its yield peak is obviously broader.[52,53] PP-A starts an early plateau (about 25% strain) than PP-B (about 40% strain), indicating that the deformation of PP-B is more homogenous than PP-A.[54] On the other hand, the elongation at break of PP-B (116.5%) is about 38% higher than that of PP-A (78.7%), indicating a superior ductility of PP-B, which might also be attributed to the presence of higher proportion of β-form and less amount of structural defects in PP-B.

Morphological Evolution of the Samples During the Stretching

To delve into the influence of the stereo-defect distribution on the morphology evolution and tensile behavior of the samples in this study, SEM, DSC, WAXD are carried out. The injection-molded specimens are loaded with a cross-head speed of 5 mm/min (strain rates 0.001/s) stretching 0, 12.5%, 25%, 50%, and 75% respectively.

SEM Analysis. In this section, two-direction SEM observations after etching, the perpendicular to the stretching direction(TD)

Table III. Crystalline Structure Parameters of PP-A and PP-B Samples Containing 0.3 wt % WBG-II Obtained from WAXD

Parameters	Sample	(110)α	(300)β	(041)α
2θ (°)	PP-A	13.897	15.802	20.904
	PP-B	13.803	15.744	20.738
d-spacing (A)	PP-A	6.3670	5.6035	4.2459
	PP-B	6.4103	5.6243	4.2796
L (nm)	PP-A	6.3	8.8	5.2
	PP-B	6.7	8.9	5.6
$K_{\beta\text{-WAXD}}$ (%)	PP-A		53.4	
	PP-B		69.8	

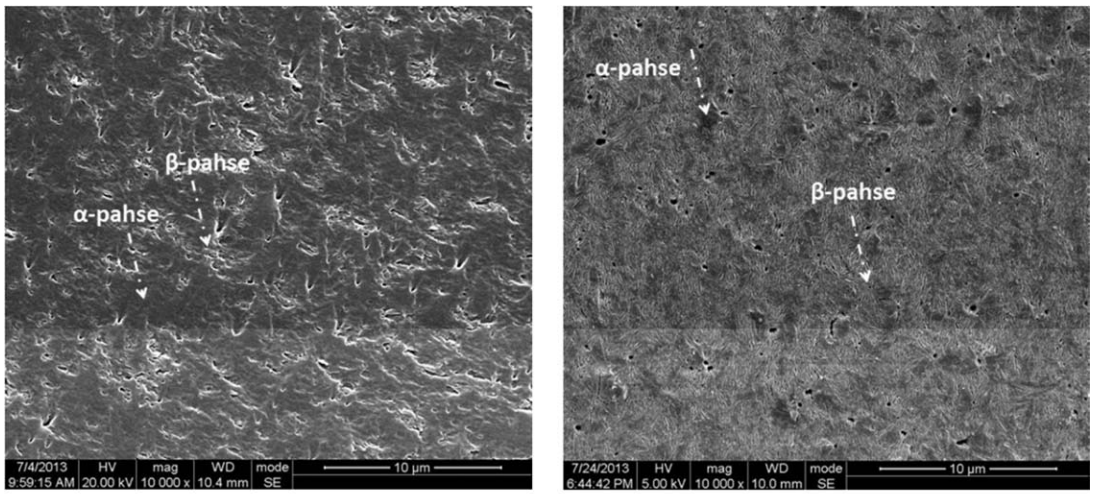

Figure 4. SEM photographs of (a) PP-A and (b) PP-B injection molding samples containing 0.3 wt % WBG-II (magnification = 10,000×).

and parallel to the stretching direction(MD) [as is illustrated in Figure 6(a)], are performed and the obtained results of PP-A and PP-B are shown in Figure 6(b,c), respectively.

It can be seen in the Figure 6(b) that for PP-A, when the tensile strain is 12.5%, the lamellaes are deformed and elongated along MD, and some small cavities emerge at the TD direction; As the strain increases to 25%, the cavities can be observed in both MD and TD direction, which might be the result of the further separation and deformation (stripping, glide, rotation, rupture, etc.) of the lamellaes. This phenomenon is found to be helpful for dispersing the stress and for preservation of the crystalline structures; When the strain increases to 50%, the original crystal morphology of PP-A is completely destroyed, the crystals are broken and begin to reorient along the MD, meanwhile, a plenty of cavities have formed both in MD and TD; When the strain is 75%, the density of cavities in MD direction begin to decrease drastically, which might correspond the destruction of the lamellaes and "close" of the formed cavities.[55] Meanwhile, the density of cavities in TD direction continuously increases. Generally, it can be seen that a combination deformation consisting of both the lamellar deformation (lamellae break up and reorientation) and amorphous (i.e., lamellar separation and formation of voids) takes place in PP-A.

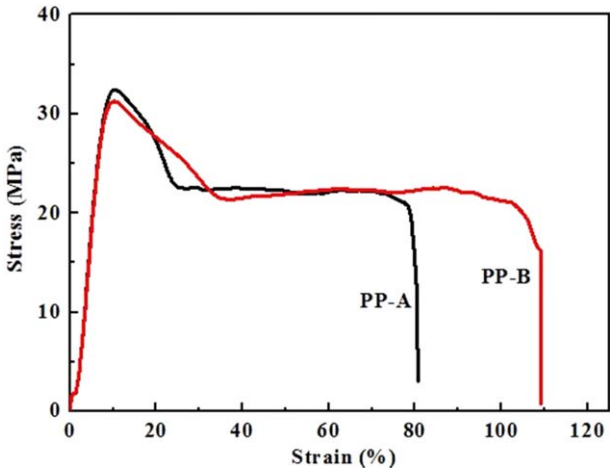

Figure 5. Stress–strain curves for PP-A and PP-B injection-molded samples with 0.3 wt % WBG-II. [Color figure can be viewed in the online issue, which is available at wileyonlinelibrary.com.]

On the other hand, Figure 6(c) shows that for PP-B, when the strain is 12.5%, many small cavities emerge in the TD direction and distribute uniformly, indicating that more amount of lamellae separation (namely, the amorphous deformation) take place; as the strain increases to 25%, it can be seen that the lamellaes deform in a more uniform manner compared with PP-A, meanwhile, the number of cavities in TD increases, which distribute uniformly; At the strain of 50%, and more amount of cavities with large sizes can be observed in both TD and MD directions, indicating that at this stage, the original morphology is totally destructed, and the lamellaes are highly separated. The differences in the morphologies of PP-A and PP-B at this stage might explain their different elongation at break: with higher degree of amorphous deformation and lamellae separation, PP-B has higher capability to transmit and disperse the stress, resulting in a better ductile and higher elongation at break. When the strain increases to 75%, unlike PP-A, there still exist large amount of cavities in PP-B, indicating the preservation of large amount of lamellae structures in MD and TD, that is to say the presence of large amount of cavities structure, and the crystalline structures are preserved to a large extent.

Table IV. Tensile Parameters of PP-A and PP-B

Sample	Yield strength (MPa)	Elasticity modulus (MPa)	Elongation at break (%)
PP-A	32.4 ± 0.2	478 ± 7	78.7 ± 6.5
PP-B	31.6 ± 0.1	451 ± 6	116.5 ± 4.9

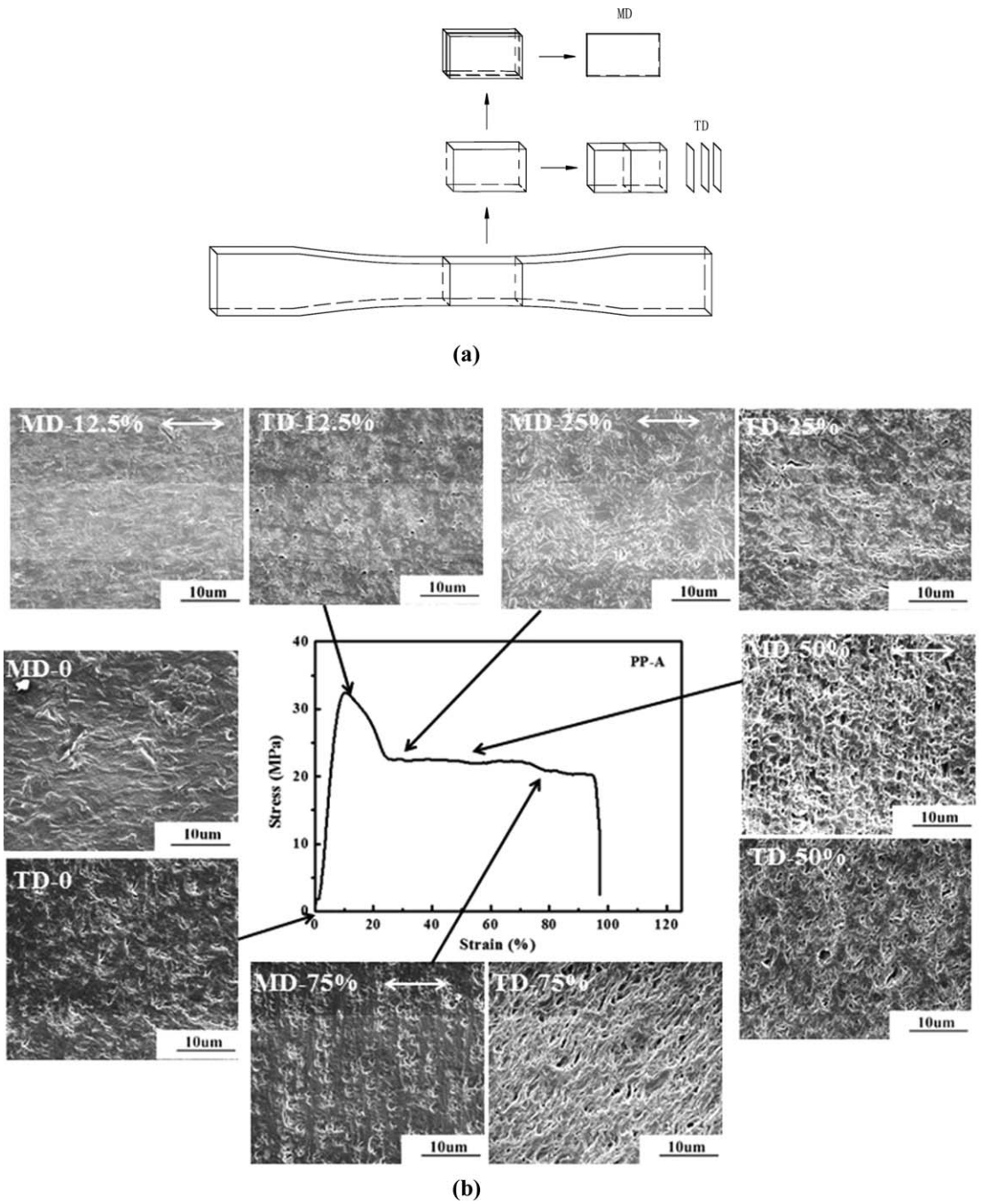

Figure 6. (a) SEM images along the drawing direction (MD) and transverse direction (TD) of etched injection-molded samples of (b) PP-A and (c) PP-B with 0.3 wt % WBG-II at varied strains (magnification = 10,000×). The white arrows show the tensile direction.

WAXD Analysis. To further the understanding of the morphology and orientation evolution behavior of the samples, 2D-WAXD is performed. The 2D-WAXD patterns are taken from the core layer after removing the molding-induced skin layers by polishing, presented in Figure 7. The images are on the same logarithmic scale.

As can be seen from the diffraction patterns, before deformation, the intensity of (110)α plane (the inner ring) of PP-A is stronger than that of PP-B, indicating a higher α-phase content in PP-A, which is consistent with previous analysis. When the strain is 25%, a more concentrated outer ring is observed in PP-A, indicating that the orientation in PP-A is more obvious compared with PP-B. As the strain gradually increases to 75%, all the rings are gradually concentrated, indicating the increase of orientation in PP-A and PP-B under tensile stress. Interestingly, an important difference between PP-A and PP-B should be noticed. For strain-0 samples, the (300)β (the second inner ring) intensity of PP-B is stronger than that of PP-A. As the strain increases, the (300)β intensity of PP-A gradually becomes weaker, indicating a sharp decrease of β-phase under the tensile

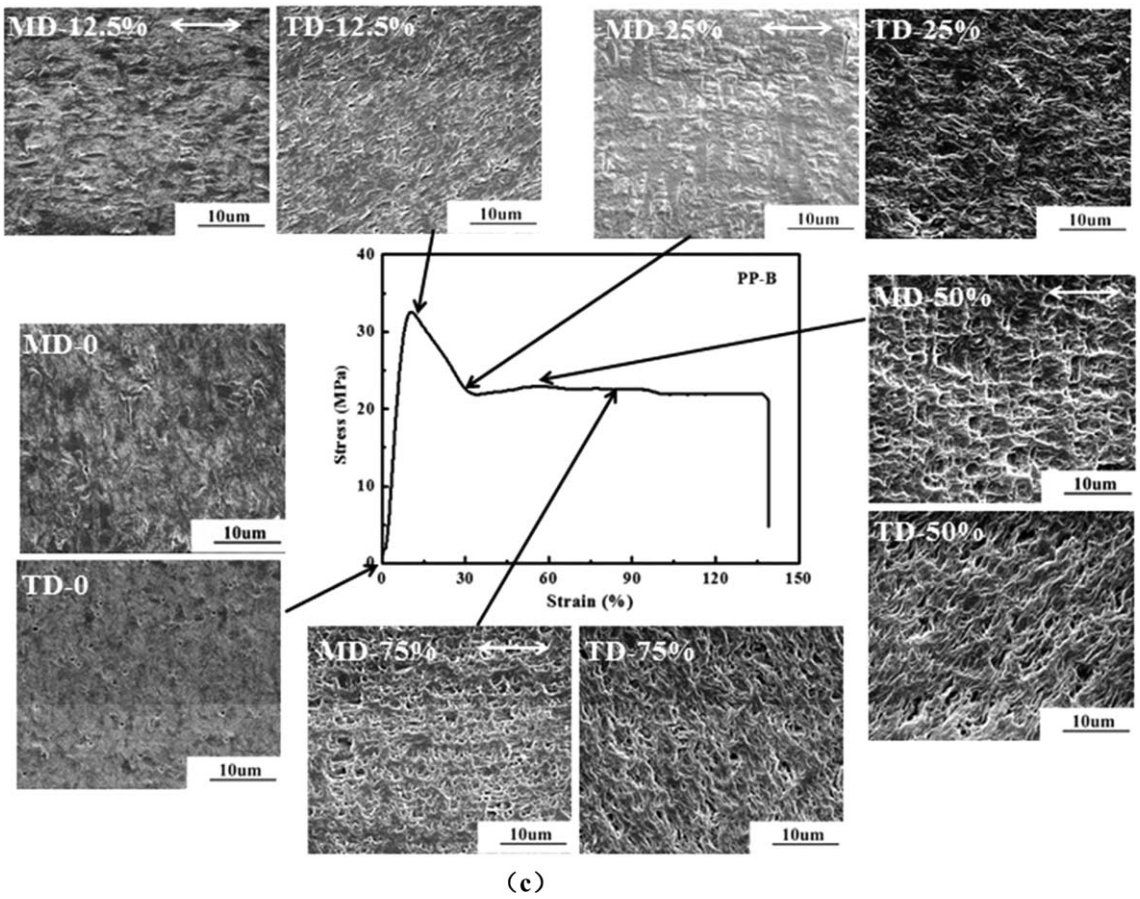

(c)

Figure 6. (Continued)

stress in PP-A, which might correspond to the deformation and fragmentation of the β-crystals; meanwhile, the strong (300)β ring of PP-B remains sharp and decrease more slowly as the strain increases, which might suggest that in PP-B, the β-lamellaes are less deformed and destroyed under the tensile stress, compared with PP-A.

To understand fully, the 1D-WAXD profiles of the samples are calculated from Figure 7, as shown in Figure 8. From Figure 8 one can see that, the WAXD profiles of PP-A and PP-B show the typical characteristic diffractions at $2\theta = 16.1°$, $21.1°$, indicating the presence of the (300) and (301) planes of β-iPP, respectively. Furthermore, some important characteristic

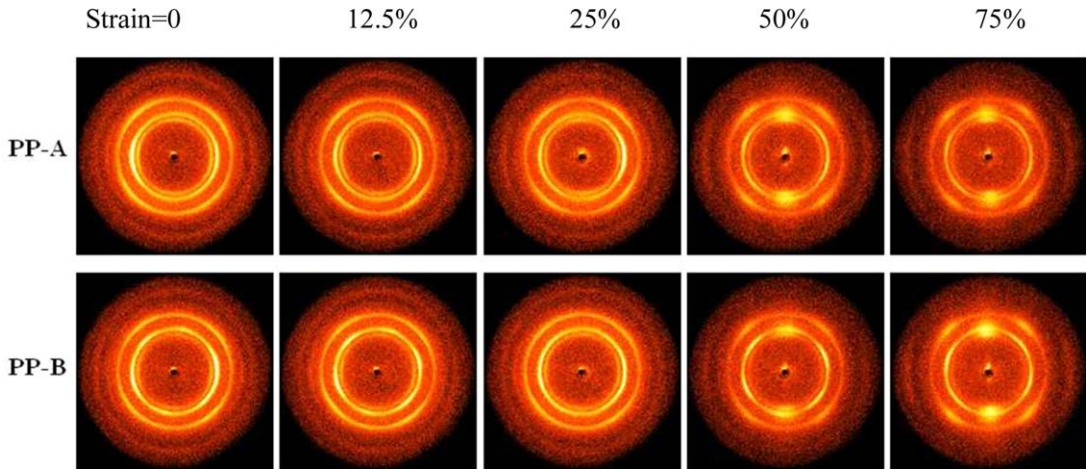

Figure 7. 2D-WAXD patterns of the injection-molded samples of PP-A and PP-B with 0.3 wt % WBG-II during uniaxial tensile deformation at room temperature. [Color figure can be viewed in the online issue, which is available at wileyonlinelibrary.com.]

diffraction peaks of the α-iPP can be differentiated at $2\theta = 14.2°$ (110), 18.7° (130).[46] Moreover, the relative percentage of β-phase, $K_{\beta\text{-WAXD}}$ of the samples are calculated and plotted in Figure 9, as a function of tensile strain. Figure 10 depicts the melting curves of the samples at varied strains.

As can be seen from Figure 9, the $K_{\beta\text{-WAXD}}$ of PP-A and PP-B gradually decreases with the development of deformation, and $K_{\beta\text{-WAXD}}$ of PP-B is higher at all strains compared with its counterpart of PP-A. As the strain increases from 25 to 50%, a significant drop of $K_{\beta\text{-WAXD}}$ can be observed in PP-A, while only small decrease of $K_{\beta\text{-WAXD}}$ can be seen for PP-B. As the strain reaches 75%, the $K_{\beta\text{-WAXD}}$ of remained β-phase of PP-B is obviously higher than that of PP-A. On the other hand, the peak of (110)α is higher for PP-A at all strains, compared with its counterpart of PP-B. As the strain increases, the intensity of this peak of PP-A decreases significantly, while in PP-B, only mild decrease of (110)α peak can be observed. Meanwhile, the results of DSC in Figure 10 show that the content of β-phase of PP-B is higher than PP-A at the same strain, which is in accord with the results of 1D-WAXD.

The above differences of the variation trends of (300)β ($K_{\beta\text{-WAXD}}$) and (110)α of PP-A and PP-B are attributed to the differ-

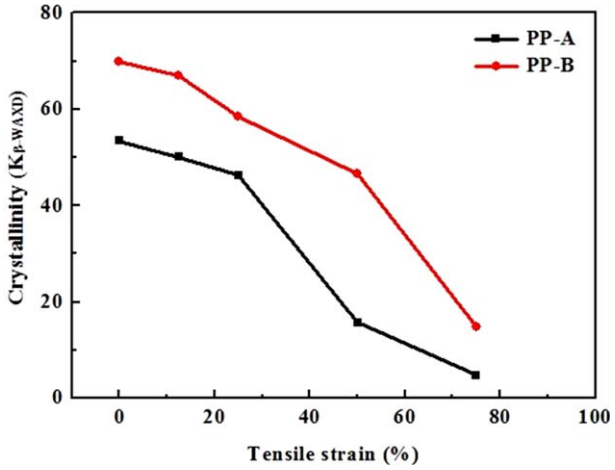

Figure 9. Plots of $K_{\beta\text{-WAXD}}$ as a function of tensile strain of injection-molded samples of PP-A and PP-B with 0.3 wt % WBG-II. [Color figure can be viewed in the online issue, which is available at wileyonlinelibrary.com.]

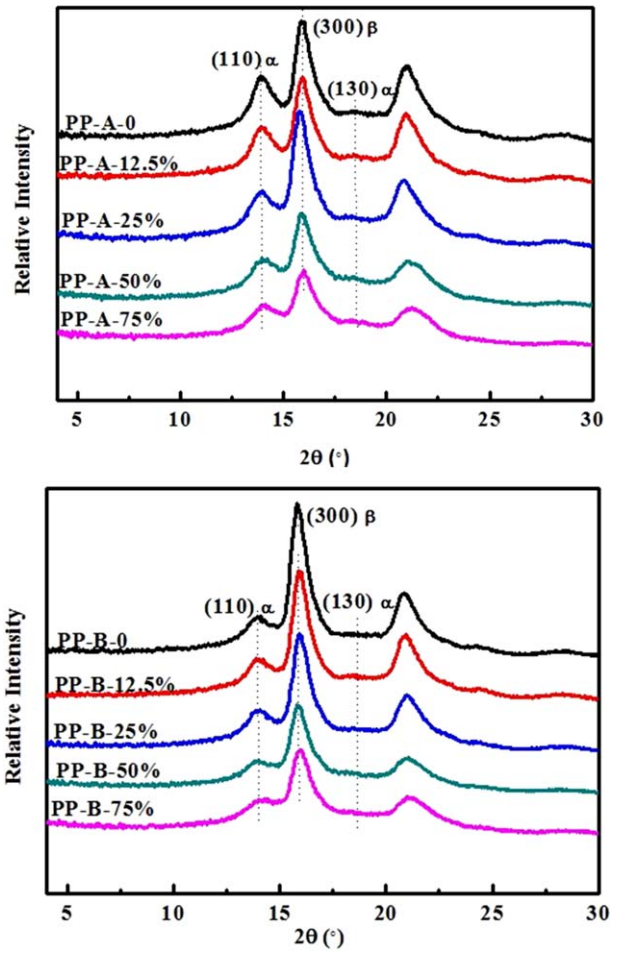

Figure 8. 1D-WAXD patterns of PP-A and PP-B injection-molded samples with 0.3 wt % WBG-II during the drawing process. [Color figure can be viewed in the online issue, which is available at wileyonlinelibrary.com.]

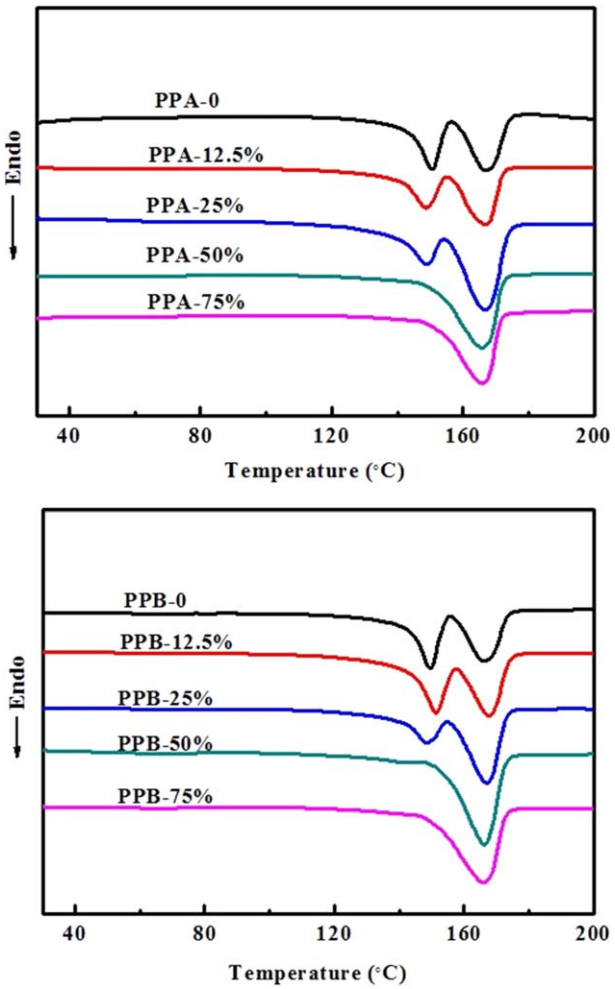

Figure 10. DSC melting curves of (a) PP-A and PP-B injection-molded samples containing 0.3 wt % WBG-II during the drawing process. [Color figure can be viewed in the online issue, which is available at wileyonlinelibrary.com.]

ent morphologies of the sample. For PP-A, since there exist more amount of defective structures and less amount of β-phase, both the lamellar deformation and amorphous deformation take place, resulting in a significant destruction of the crystallines structures (including both α- and β-phase) as the strain increases, and a lower elongation at break; For PP-B, with more amount of β-phase and higher crystalline perfection, an amorphous deformation (lamellar separation and relative mild lamellar deformation) is more preferred to occur. With the help of cavitation and amorphous deformation, the tensile stress can be better transmitted and dispersed, meanwhile, the crystalline structures can be preserved in a larger extent, compared with PP-A. Therefore, PP-B still has obviously higher amount of β-phase when the stain reaches to 75%, and has longer elongation at break and ductile property.

From the results above, it can be concluded that under the processing condition of injection molding, the morphology of β-PP samples nucleated by WBG-II with different uniformities of stereo-defect distribution exhibit quite different morphologies and tensile behavior. For PP-A with less uniform distribution of stereo-defect, it has strong ability for the formation of α-phase [40]. Under the influence of WBG-II and the processing condition of injection molding, PP-A is not favorable for the formation of large amount of β-phase, and only a mixture of α- and β-phase with many defective structures can be obtained. On the other hand, PP-B with more uniform stereo-defect distribution is more favorable for the formation of high proportion of β-phase, under the same condition. Therefore, in the design of structure-properties of the β-PP products, the uniformity of stereo-defect distribution is an important factor which must be taken into consideration.

CONCLUSIONS

In this study, two β-PP injection-molded samples with different uniformities of stereo-defect distribution, nucleated by 0.3 wt % WBG-II, were prepared, and their morphologies, tensile behaviors and morphology evolutions were studied using SEM, DSC and 2D-WAXD. The following conclusions can be drawn.

Under the influence of WBG-II and injection molding processing, PP-A with less uniform stereo-defect distribution is favorable for the formation of the mixture structure of α- and β-crystals and relative low structural perfection. During room temperature stretching, both the lamellar separation (amorphous deformation) and lamellar deformation take place, and only relatively low amount of cavitation is observed. Finally, the elongation at break of PP-A is relatively low.

Under the same conditions, PP-B with more uniform stereo-defect distribution is more favorable for the formation of relative large amount of β-crystals with relative high structural perfection. During the tensile test, the lamellar separation mainly takes places and large amount of cavitation is observed. The β-phase content decreases slowly as the strain increases, and the elongation of PP-B is higher. Generally, in the design of structure-properties of the β-PP products, the uniformity of stereo-defect distribution is an important factor which must be taken into consideration.

ACKNOWLEDGMENTS

The authors thank the Sichuan University Scientific Research Foundation for Young Teachers (2012SCU11075) and National Science Foundation of China (NSFC 51203106) for their support.

REFERENCES

1. Thomann, R.; Semke, H.; Maier, R. D.; Thomann, Y.; Scherble, J.; Mulhaupt, R.; Kressler, *J. Polymer* **2001**, *42*, 4597.
2. Auriemma, F.; de Rosa, C.; Boscato, T.; Corradini, P. *Macromolecules* **2001**, *34*, 4815.
3. VanderHart, D. L.; Alamo, R. G.; Nyden, M. R.; Kim, M. H.; Mandelkern, L. *Macromolecules* **2000**, *33*, 6078.
4. Meille, S. V.; Bruckner, S.; Porzio, W. *Macromolecules* **1990**, *23*, 4114.
5. Alamo, R. G.; VanderHart, D. L.; Nyden, M. R.; Mandelkern, L. *Macromolecules* **2000**, *33*, 6094.
6. Foresta, T.; Piccarolo, S.; Goldbeck-Wood, G. *Polymer* **2001**, *42*, 1167–1176.
7. de Rosa, C.; Auriemma, F.; Circelli, T.; Waymouth, R. M. *Macromolecules* **2002**, *35*, 3622.
8. Liu, M. X.; Guo, B. C.; Du, M. L.; Chen, F.; Jia, D. M. *Polymer* **2009**, *50*, 3022.
9. Hoyos, M.; Tiemblo, P. Gómez-Elvira, J. M. *Eur. Polym. J.* **2009**, *45*, 1322.
10. Somani, R. H.; Hsiao, B. S.; Nogales, A.; Srinivas, S.; Tsou, A. H.; Sics, I. *Macromolecules* **2000**, *33*, 9385.
11. Somani, R. H.; Hsiao, B. S.; Nogales, A.; Srinivas, S.; Ezquerra, T. A. *Macromolecules* **2010**, *33*, 9385.
12. Yamamoto, Y.; Inoue, Y.; Onai, T.; Doshu, C.; Takahashi, H.; Uehara, H. *Macromolecules* **2007**, *40*, 2745.
13. Yi, Q. F.; Wen, X. J.; Dong, J. Y.; Han, C. C. *Polymer* **2008**, *49*, 5053.
14. Padden, F. J.; Keith, H. D. *J. Appl. Phys.* **1959**, *30*, 1479.
15. Padden, F. J.; Keith, H. D. *J. Appl. Phys.* **1959**, *30*, 1485.
16. Byelov, D.; Panine, P.; Remerie, K.; Biemond, E.; Alfonso, G. C. *Polymer* **2008**, *49*, 3076.
17. Ellis, G.; Gomez, M. A.; Marco, C. *J. Macromol. Sci. Phys.* **2005**, *43*, 191.
18. Zhou, J.; Liu, G.; Yan, S.; Dong, J.; Li, L.; Chan, C. *Polymer* **2005**, *46*, 4077.
19. Huo, H.; Jiang, S. C.; An, L. J.; Feng, J. C. *Macromolecules* **2004**, *37*, 2478.
20. Varga, J. *J. Macromol. Sci. Part B: Phys.* **2002**, *41*, 1121.
21. Varga, J.; Menyhard, A. *Macromolecules* **2007**, *40*, 2422.
22. Seguela, R. *Macromol. Mater. Eng.* **2007**, *292*, 235.
23. Humbert, S.; Lame, O.; Vigier, G. *Polymer* **2009**, *50*, 3755.
24. Humbert, S.; Lame, O.; Chenal, J. M.; Rochas, C.; Vigier, G. *Macromolecules* **2010**, *43*, 7212.
25. Van-Pham, D. T.; Sorioka, K.; Norisuye, T. Tran-Cong-Miyata, Q. *Polymer* **2011**, *52*, 739.

26. Galeski, A.; Bartczak, Z.; Kazmierczak, T.; Slouf, M. *Polymer* **2010**, *51*, 5780.
27. Liu, G. M.; Guan, Y.; Wen, T.; Wang, X. W.; Zhang, X. Q.; Wang, D. J. *Polymer* **2011**, *52*, 5221.
28. Luo, F.; Geng, C. G.; Wang, K.; Deng, H.; Chen, F.; Fu, Q. *Macromolecules* **2009**, *42*, 9325.
29. Zhang, X. D.; Shi, G. Y. *Thermochim. Acta* **1994**, *235*, 45.
30. Kang, J.; Cao, Y. *J. Polym. Res.* **2012**, *19*, 1.
31. Kang, J.; Gai, J. G.; Xiang, M. *J. Polym. Res.* **2013**, *20*, 1.
32. Lucia, F. B.; Thurman, D. W.; Zhou, W. J.; Julia, A. *Macromolecules* **2012**, *45*, 6557.
33. Stribeck, N.; Zeinolebadi, A. *Macromolecules* **2012**, *45*, 962.
34. Ruiz-Orta, C.; Juan, P.; Amelia, M. *Macromolecules* **2011**, *44*, 3436.
35. Kang, J.; Cao, Y.; Xiang, M. *Eur. Polym. J.* **2012**, *48*, 425.
36. Nyden, M. R.; Vanderhart, D. L.; Alamo, R. G. *Comput. Theor. Polym. Sci.* **2011**, *11*, 175.
37. Rosa, C. D.; Auriemma, F. *J. Am .Chem. Soc.* **2004**, *126*, 17040.
38. Alamo, R. G.; Blanco, J. A.; Agarwal, P. K.; Randall, J. C. *Macromolecules* **2003**, *36*, 1559.
39. Randall, J. C.; Alamo, R. G.; Agarwal, P. K.; Ruff, J. C. *Macromolecules* **2003**, *36*, 1572.
40. Kang, J.; Chen, J. Y.; Cao, Y.; Li, H. L. *Polymer* **2010**, *51*, 249.
41. Kang, J.; Li, H. L.; Cao, Y.; Xiang, M. *J. Appl. Polym. Sci.* **2013**, *130*, 25.
42. Kang, J.; Yang, F.; Cao, Y.; Li, H. L.; Xiang, M. *J. Appl. Polym. Sci.* **2012**, *125*, 3076.
43. Kang, J.; Cao, Y.; Li, H. L.; Yang, F.; Xiang, M. *J. Appl. Polym. Sci.* **2013**, *129*, 2663.
44. Li, J. X.; Cheung, W. L.; Jia, D. *Polymer* **1999**, *40*, 1219.
45. Olley, R. H.; Bassett, D. C. *Polymer* **1982**, *23*, 1707.
46. Turner Jones, A.; Aizlewood, J. M.; Beckett, D. R. *Macromol. Chem.* **1964**, *75*, 134.
47. Menyhárd, A.; Varga, J. *Eur. Polym. J.* **2006**, *42*, 3257.
48. Scudla, J.; Raab, M.; Eichhorn, K. J.; Strachota, A.; *Polymer* **2003**, *44*, 4655.
49. Kotek, J.; Kelnar, I.; Baldrian, J.; Raab, M. *Eur. Polym. J.* **2004**, *40*, 679–684.
50. Li, J. X.; Cheung, W. L.; Chan, C. M. *Polymer* **1999**, *40*, 2089.
51. Li, J. X.; Cheung, W. L.; Chan, C. M. *Polymer* **1999**, *40*, 3641.
52. Chen, H. B.; Karger-Kocsis, J.; Wu, J. S.; Varga, J. *Polymer* **2002**, *43*, 6505.
53. Varga, J. *J. Macromol. Sci. Phys.* **2002**, *41*, 1121.
54. Bai, H. W.; Luo, F.; Zhou, T. N.; Fu, Q. *Polymer* **2011**, *52*, 2351.
55. Ran, S. F.; Xu, M. *Chin. J. Polym. Sci.* **2004**, *22*, 123.